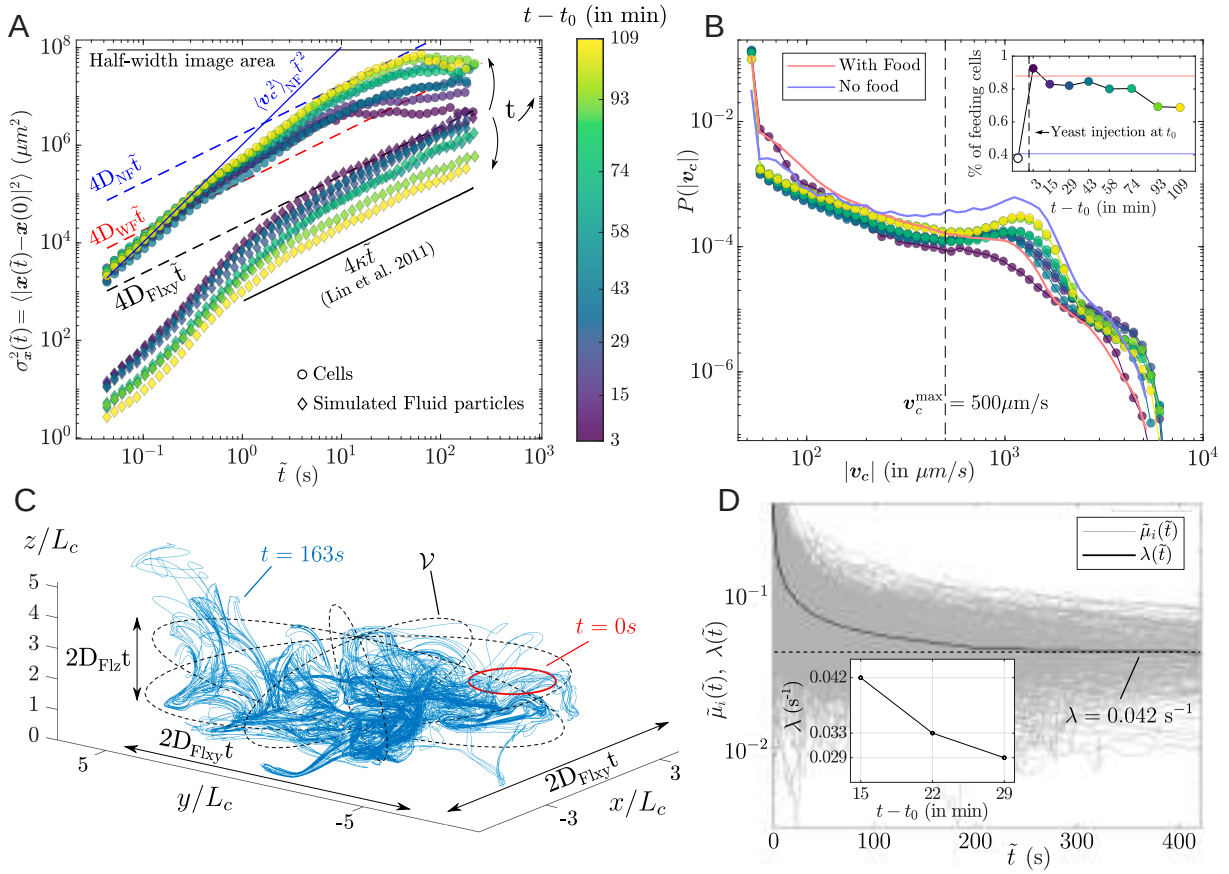

Fig. 5. (*A*) Temporal evolution of the MSDs $\sigma^2_{\tilde{\boldsymbol{x}}}(\tilde{t})$ for both cells and tracers. Each curve is computed over $\tilde{t} \in [0, T]$, at multiples of $(t - t_0) \approx 15$ min, with t_0 the injection time. They are compared to the asymptotic MSDs (dashed lines) extracted from Fig. 1*G* for cells evolving in homogeneous environments (either no-food or with-food conditions), as well as to the model of dispersion by squirmers (42), depicted as a continuous black line. (*B*) $P(|\boldsymbol{v_c}|)$ at successive times $(t - t_0)$ [same colorbar as in (*A*)] and compared to the homogeneous cases from Fig. 1*H*. *Inset*: Proportion of feeding cells over the total number of cells, computed as the fraction of cells with a locomotion velocity $v_c < v_c^{\max}$. (*C*) Material points (tracers) initially arranged on a circle (in red) of length l_0 are advected by the collective flow. After $t = 165$ s the circle is stretched exponentially up to $\rho = l/l_0 \approx 650$ into the blue material line [computed using the Diffusive Strip Method (49)]. (*D*) Temporal evolution of $\tilde{\mu}_i(\tilde{t})$, and their average $\lambda(\tilde{t})$, converging to the value $\lambda \approx 0.042\,\mathrm{s}^{-1}$, for the movie at $t - t_0 = 15$ min. *Inset*: λ values for the three successive movies at early times $t - t_0 = [15, 22, 29]$ min.

that is about 30 times smaller than $D_{Flxy} = 6.10^{-9}\,\mathrm{m}^2/\mathrm{s}$. This stark contrast confirms the much higher fluid transport efficiency of *S. lemnae*'s collective feeding flows compared to their crawling-induced flow. Additionally, note that κ is probably overestimated, as the model by Lin et al. (42) ignores effects of the no-slip wall that increase velocity fluid decay from $v \sim 1/r^2$ to $v \sim 1/r^3$.

Finally, we find that food spreading is even faster when the feeding cluster is already established. We performed the simple experiment of a second yeast injection near an existing feeding cluster formed by a prior injection (*SI Appendix*, section 13A and Movie S17). From the second injection time, we computed both cell and tracer MSDs as in Section 5 (*SI Appendix*, section 13B). While cell MSDs display a subdiffusive behavior indicative of some chemotactic response, tracer MSDs exhibit a persistent superdiffusive regime over 2.5 decades in time as $\sigma^2_{\boldsymbol{x}} = \langle|\boldsymbol{x}(t) - \langle\boldsymbol{x}(t)\rangle|^2\rangle \sim t^{1.6}$. This anomalous scaling reflects persistent hydrodynamic interactions, which enhance food transport efficiency via preferential flow paths.

5.2. Fluid Stretching. Fluid dispersion is linked here to chaotic mixing. Indeed, while feeding, *S. lemnae* continues to perform stochastic reorientations. In this way, the 2D manifolds acting as barriers to transport are regularly destroyed while new ones are built. The ensuing unsteady flow imparts stretching and folding of the fluid elements, the hallmark of chaotic advection most favorable to fluid mixing (51), which we quantify here. For example, Fig. 5*C* illustrates how an initial material line is stretched exponentially by the collective flow into a complex lamellar structure (Movie S18). To quantify the deformation rate, we typically compute the infinite-time Lyapunov exponent, defined as the median stretching rate $\lambda = \lim_{t\to\infty} \ln \rho(t)/t$ with $\rho(t) = l(t)/l(0)$ and $l(t)$ the length of the material line. However, in open flows $\lambda = 0$. Indeed, at some time all fluid particles will be expelled along z out of the influence zone of the pumping flow, where velocity fluctuations vanish. In other words, the unstable manifold is not space-filling anymore but has a fractal dimension, prior to escaping the influence zone (52, 53), that we call mixing region. Consequently, we rather compute the average of the finite-time Lyapunov exponents (FTLEs), evaluated along trajectories as long as they remain inside the mixing region. We define the mixing region as the volume delimited by the minimal envelope surrounding the evolving feeding cluster in the xy plane, and by a height limit $z_{\lim}$ (*SI Appendix*, section 14). Choosing $z_{\lim}$ is delicate as it sets the limit of integration of the FTLEs which decay with z. We set $z_{\lim} = 20h$ based on the measurement that only 8% of the fluid particles are lost beyond $z_{\lim}$ after the $T = 3.5$ min duration of the movie taken at $t - t_0 = 15$ min, implying that the defined mixing region captures nearly all

Lagrangian kinematics over that period (*SI Appendix*, Fig. S13*B* and Fig. 5*C*). Regarding the movie $t-t_0 = 15$ min, we compute FTLEs $\tilde{\mu}_i(\tilde{t})$ along trajectories i within the mixing region, and take their average $\lambda(\tilde{t}) = \langle\tilde{\mu}_i(\tilde{t})\rangle$. Fig. 5*D* shows convergence to $\lambda \approx 0.042\,\mathrm{s}^{-1}$ after $\tilde{t} = 2T$ (see *SI Appendix*, section 15 for further details about FTLEs computation, and Movie S19). This convergence was also achieved for three successive movies at early times $t-t_0 = [15, 22, 29]$ min (note that we incorporate here the movie $t-t_0 = 22$ min, not considered in the previous section), as can be observed on the *Inset* of Fig. 5*D* which shows a decay of λ in time, in parallel to the regular decay of the MSDs for the fluid particles. Here too, the decay of λ over time results from fewer cells contributing to the collective flow. Last, the Lyapunov exponent λ is made dimensionless as $\lambda\tau_c$, where τ_c is the average feeding period between fast crawling events (i.e. for which $v_c < v_c^{\max}$). Regarding the movie $t-t_0 = 15$ min, we find $\tau_c \approx 2.1$ s, yielding a dimensionless Lyapunov exponent $\lambda\tau_c \approx 0.09$. The dimensionless λ enables comparison of the chaotic strength of the collective flow to known passive laminar chaotic flows and to notice that *S. lemnae* performs well (for the given mixing region): less than random porous media [$\lambda \approx 0.21$ (54)], or sheared particulate suspension [$\lambda \approx 0.21$ for a solid volume fraction of $\phi = 0.35$ (55)], but better than ordered porous media [$\lambda \approx 0.073$ (56)].

5.3. Mixing Time and Coalescence Time. We provide here characteristic times indicative of the fluid mixing rate by the collective flow, using the lamellar approach (35, 49). This theoretical framework describes evolving concentration fields as a set of stretched filaments (lamellae), where the concentration within each lamella is governed by the coupling between its stretching history ρ and molecular diffusion D. In 3D flows, mixtures form 3D sheets whose material area elements align with the principal strain directions, while the compression direction lies mainly perpendicular to the surface (57, 58). Fluid incompressibility dictates that the sheet width decays as ρ^{-1}, until enhanced diffusion and compression balance the sheet width down to the Batchelor scale s_b, corresponding to the mixing time t_s. In chaotic flows, 3D sheets experience a constant elongation rate on average $\dot{\rho}/\rho = \lambda$ so that $\rho \sim e^{\lambda t}$. In such a case, s_b remains constant over time as $s_b = \sqrt{D/\lambda}$, at the mixing time $t_s = (1/2\lambda)\ln(1+2Pe)$. Of course, in our open flow, the parameters s_b, λ and so t_s are in reality space-dependent, varying on average as a function of z. Here, we focus on averages within the mixing region. Taking $\lambda = 0.042\,\mathrm{s}^{-1}$, and $D_{\mathrm{yeast}} = 10^{-11}\,\mathrm{m}^2/\mathrm{s}$, we get $t_s \approx 80$ s. By contrast, purely diffusive mixing of a $s_0 = 500\,\mu$m-thick blob in a still ambient fluid would take $t_s \approx s_0^2/D_{\mathrm{yeast}} = 2.5\times10^4$ s, illustrating how powerful exponential stretching is to accelerate dilution. Later, coalescence of the sheets further accelerate homogenization. Initially well separated, the adjacent sheets inevitably merge as the unfolded blob volume expands faster than the surrounding dispersion volume (35, 59). Since the sheet surface grows exponentially while its thickness is locked at s_b, the unfolded blob volume V in turn increases exponentially as

$$V \sim \frac{4}{3}\pi s_b s_0^2 e^{\lambda t}, \qquad [4]$$

with s_0 the initial blob radius. Meanwhile, the blob is bounded by the dispersion envelope (see scheme of Fig. 5*C*) growing as a power law:

$$\mathcal{V} \sim \frac{4}{3}\pi(s_0^2 + 2D_{Flxy}t)\sqrt{s_0^2 + 2D_{Flz}t} \sim t^{3/2}, \qquad [5]$$

with D_{Flxy} and D_{Flz} computed earlier. The average number of overlaps is given by the ratio $V/\mathcal{V}$. The time at which the lamellae overlap once on average $V/\mathcal{V} = 1$ is referred to as the coalescence time, and for the movie $t-t_0 = 15$ min corresponds to $t_{\mathrm{coal}} \approx 150$ s (*SI Appendix*, Fig. S15). Coalescence further accelerates homogenization toward the mean concentration $\langle C\rangle = C_0/\mathcal{V}$. Importantly, both mixing and coalescence times occur very early compared to the lifespan of the feeding cluster (~1 to 2 h in the present case), underscoring the efficiency of the collective flow in mixing solutes. Also, if some fluid is constantly expelled from the mixing region and exchanged with fresh fluid, at $t_{\mathrm{coal}} = 150$ s only 6% of the fluid particles have left the mixing region (*SI Appendix*, Fig. S12*B*). This suggests that, already at $t-t_0 = 15$ min, most cells within the cluster should probe a similar concentration of food or nutrients. Additionally, a cell arriving at the edge of an already established feeding cluster has in an instant a fair appreciation of the chemical content of the mixing region.

6. Discussion

By organizing into feeding clusters, *S. lemnae* gains the ability to spread and mix fluid over larger scales. One can legitimately ask whether this organization provides benefits to *S. lemnae*, and at what cost: In other words, is the feeding cluster of a cooperative nature? At present, in laboratory conditions, improved foraging success is a potential benefit emerging from our results. It arises from two mechanisms. First, the active spreading of food—driven by and along with the formation of an expanding feeding cluster—increases the probability that still-foraging cells encounter food, scaling with the patch surface as $S \sim \sigma_x^2 \sim D_{Flxy}t$. Second, once a feeding cluster is established, it gains the ability to spread any neighborhood food source even faster throughout the cluster, with superdiffusive scaling $S \sim \sigma_x^2 \sim t^{1.6}$. Both mechanisms hasten the spatial overlap between the distributions of cells and food, increasing the probability of interactions between them. Whether this increased probability of interaction actually leads to an enhanced feeding efficiency per cell within the group remains a compelling hypothesis to be tested by future studies. Furthermore, it is not yet known to what extent these enhanced interactions apply under natural conditions, for example if cells crawl on more complex solid surfaces or are exposed to external flows.

As for the costs of maintaining collective flows, our preliminary estimate is that they are not significant. As mentioned above, collective flows arise primarily from the reduction in locomotion speed v_c of cells clustered around a food patch. Modulating locomotion velocity is a well-known chemotactic strategy that is sufficient to explain the individual behavior of cells. Furthermore, near a food patch, *S. lemnae* behaves similarly whether isolated or as part of a cluster. In all cases, it remains in the food patch, its feeding flow does not weaken and persists beyond cell satiety. The most notable distinction arises from the physical contacts that inevitably occur as cells cluster together. These contacts elicit avoidance reactions, which manifest as SSR moves that may propagate across the population. Far from having a negative impact, this effect could help maintain minimal spacing between cells, allowing for more efficient spatial coverage by the cluster. Whether this phenomenon represents a form of self-organization will be the subject of future research. Regarding the collective flow itself, while it is true that its dilution effect could be counterproductive in terms of feeding efficiency if the initial concentration were low, this is not a concern here given the initially high concentration.

Thus, since potential benefits appear to outweigh costs, we believe that the feeding cluster represents a form of cooperative behavior employed by *S. lemnae*. Until further investigation uncovers more active forms of cooperation such as active signaling or enhanced feeding rates per cell, we recognize here a type of intraspecific cooperation termed by-product cooperation. Such cooperation could apply to other Spirotrich species, as we have observed similar behavioral patterns in *S. mytilus* and *Euplotes vannus*. More broadly, the hydrodynamic cooperation observed in *S. lemnae* shares striking similarities with that of previously cited organisms, namely *T. majus* and *Uronemella* (29–31): In all cases, clusters form in response to resource gradients, leading to long-range flows. Similarly, just as collective flows in *T. majus* and *Uronemella* depend on variations in population density driven by individual random walks, chaotic mixing in our system would not occur without stochastic reorientations of the cells. The main difference lies in the lack of physical bonds between individuals in the *S. lemnae* cluster, which likely enables them to adapt faster to dynamic environments and efficiently exploit localized ephemeral patches. In contrast, colonies such as *volvox* or choanoflagellates, which take hours to form, would be better suited for larger and persistent patches.

To help reconcile predictions of feeding rates with experimental observations for different cell organizations in a patchy food environment, as discussed in the Introduction, our results suggest that the unsteady nature of the feeder's motion may play an important role. Not only does this dynamic stochastic motion affect chemotaxis, but it also allows chaotic flows to occur, shaping resource distribution considerably. In fact, the oscillations observed between members of a *Stentor* cluster (60), the erratic contractions of *Vorticella* (10), the alternating cilia beat regime of *Oocystis asymmetrica* (18), or the stochastic and uncorrelated beating of flagella in *Salpingoeca rosetta* colonies (61), may just be additional examples of stochastic motions primarily evolved to induce chaotic flow. Future studies would benefit from incorporating cell stochastic motion into their models, as ignoring it imposes overly restrictive topological constraints on the Lagrangian kinematics and precludes chaos.

7. Conclusions and Perspectives

We described the cooperative foraging behavior of *S. lemnae* in a patchy environment. Upon discovering a food patch, *S. lemnae* reduces its locomotion speed v_c, thus increasing the range of its feeding flow. As cells cluster around the patch, individual feeding flows interact hydrodynamically, leading to a collective unsteady flow at the population scale. By combining experimental and numerical methods, we measured and predicted the full 3D unsteady flow, and quantified its transport and mixing properties. Our results show that the feeding cluster is at least 30 times more efficient at spreading fluid than a suspension of swimmers and that the Lyapunov exponent of the cluster's flow is comparable to that of known nonbiological chaotic flows. Given the potential benefits granted by collective fluid spreading and mixing without additional apparent costs, we propose that the feeding group exemplifies by-product cooperation. This study establishes a quantitative framework for understanding the highly dynamical interplay between an organism's behavior and the spatial distribution of a resource that it actively shapes. In particular, we hypothesize that optimal feeding in cell clusters in patchy environments relies more on the fluid stirring protocol than on the mere sum of individual scanning fluxes. Many aspects of a feeding cluster remain to be explored: For instance, does the cluster organization enhance the average feeding rate per cell? Could it reflect underlying coordinated cooperative behavior, such as quorum sensing driven by active chemical signaling? How might the cluster adapt to varying food properties (e.g. food dispersion coefficients), different surface architectures (like porous media), or ambient conditions (such as background flow, or confinement)? How does the cluster respond to predator repellents?

8. Materials and Methods

8.1. Cell Culture. Strains of *S. lemnae* were provided by Dieter Ammermann (Tübingen, Germany). Cultures were maintained within 10 ml of Eau Volvic at 15 °C under a 12:12 h light:dark cycle. They were fed twice a week with the alga *Chlorogonium sp.* and occasionally with yeast. Fresh cultures were established every two weeks by transferring about 30 cells into new culture medium.

8.2. Experimental Setting. Before experimentation, cells were transferred to a Petri dish and acclimated to 20 °C. Prior to each experiment, cells were starved for 24 h. Six experiments were conducted (see *SI Appendix* for details). The experiments on locomotion behavior (*SI Appendix*, section 1 and first half of *SI Appendix*, section 2) and cells dispersion (*SI Appendix*, section 5) were performed directly in their Petri dish culture, using the large field of view provided by a stereo microscope (Olympus SZX16), equipped with a Photron Fastcam Mini UX100 camera and a 0.7× or 0.8× optical objective. Experiments requiring finer spatial resolution–namely, the measurements of single flows (*SI Appendix*, section 3) and collective flow (*SI Appendix*, section 4)–were performed in an observation chamber consisting of two parallel glass plates separated by a 3 mm gap, placed on an inverted Olympus IX81 microscope. For the collective flow experiment, images were captured using a low readout-noise camera (Hamamatsu ORCA Fusion BT camera). Finally, the dye tracer experiment (*SI Appendix*, section 2) was conducted with cells in the observation chamber, and imaging performed using the Hamamatsu ORCA fusion BT camera mounted on the stereo Olympus SZX16 microscope, with a 0.8× objective.

8.3. Image Processing. Image processing was performed using in-house developed MATLAB (MathWorks) programs. Cell trajectories were reconstructed using the MATLAB PTV code by Blair and Dufresne (62). PIV analysis was performed using the PIVlab MATLAB program.

Data, Materials, and Software Availability. The data supporting the findings of the study are included in the article and in the supporting information. The raw data related to the study and the relevant MATLAB codes are available at: https://hdl.handle.net/20.500.12928/EP90AW (63).

ACKNOWLEDGMENTS. We are deeply grateful to Dieter Ammermann for providing us with *S. lemnae*. We thank Elena Di Poi for backup cultures. R.T. thanks Nicolas Salles, Nina Javerzat, Benjamin Walter, Bloen Metzger, and Henri Lhuissier for helpful discussions. We gratefully acknowledge the support by the European Research Council through the European Research Council Proof of Concept Grant Stripe-o-Morph (GA 101069436) and by the Italian Ministry of Research through the projects Response (PRIN 2020), Abyss (PRIN 2022), and Green-Swarm-Intelligence (PRO3).

Author affiliations: [a]The Biorobotics Institute, Scuola Superiore Sant'Anna, Pisa 56025, Italy; [b]Mathlab, International School for Advanced Studies, Trieste 34136, Italy; and [c]Sezione Oceanografia, Istituto Nazionale di Oceanografia e di Geofisica Sperimentale, Trieste 34151, Italy

1. T. Kiørboe, *A Mechanistic Approach to Plankton Ecology* (Princeton University Press, 2008).
2. R. Stocker, Marine microbes see a sea of gradients. *Science* **338**, 628–633 (2012).
3. J. R. Seymour, M. R. Stocker, Resource patch formation and exploitation throughout the marine microbial food web. *Am. Nat.* **173**, 02139 (2009).
4. Y. Yawata, F. Carrara, F. Menolascina, R. Stocker, Constrained optimal foraging by marine bacterioplankton on particulate organic matter. *Proc. Natl. Acad. Sci. U.S.A.* **117**, 25571–25579 (2020).
5. R. E. Breier, C. C. Lalescu, D. Waas, M. Wilczek, M. G. Mazza, Emergence of phytoplankton patchiness at small scales in mild turbulence. *Proc. Natl. Acad. Sci. U.S.A.* **115**, 12112–12117 (2018).
6. J. S. Guasto, K. A. Johnson, J. P. Gollub, Oscillatory flows induced by microorganisms swimming in two dimensions. *Phys. Rev. Lett.* **105**, 189901 (2010).
7. D. Tam, A. E. Hosoi, Optimal feeding and swimming gaits of biflagellated organisms. *Proc. Natl. Acad. Sci. U.S.A.* **108**, 1001–1006 (2011).
8. S. Michelin, E. Lauga, Optimal feeding is optimal swimming for all péclet numbers. *Phys. Fluids* **23**, 1–14 (2011).
9. R. E. Pepper *et al*., A new angle on microscopic suspension feeders near boundaries. *Biophys. J.* **105**, 1796–1804 (2013).
10. S. Ryu, R. E. Pepper, M. Nagai, D. C. France, Vorticella: A protozoan for bio-inspired engineering. *Micromachines* **8**, 1–25 (2017).
11. K. Y. Wan *et al*., Reorganization of complex ciliary flows around regenerating stentor coeruleus. *Philos. Trans. R. Soc. B Biol. Sci.* **375**, 20190167 (2020).
12. E. A. Kanso, R. M. Lopes, J. Rudi Strickler, J. O. Dabiri, J. H. Costello, Teamwork in the viscous oceanic microscale. *Proc. Natl. Acad. Sci. U.S.A.* **118**, 1–6 (2021).
13. M. Rode, T. Kiørboe, A. Andersen, Feeding flow and membranelle filtration in ciliates. *Phys. Rev. Fluids* **7**, 023102 (2022).
14. T. Kiørboe, What makes pelagic copepods so successful? *J. Plankton Res.* **33**, 677–685 (2011).
15. C. A. Solari, S. Ganguly, J. O. Kessler, R. E. Michod, R. E. Goldstein, Multicellularity and the functional interdependence of motility and molecular transport. *Proc. Natl. Acad. Sci. U.S.A.* **103**, 1353–1358 (2006).
16. M. Roper, M. J. Dayel, R. E. Pepper, M. A. Koehl, Cooperatively generated stresslet flows supply fresh fluid to multicellular choanoflagellate colonies. *Phys. Rev. Lett.* **110**, 1–5 (2013).
17. J. B. Kirkegaard, R. E. Goldstein, Filter-feeding, near-field flows, and the morphologies of colonial choanoflagellates. *Phys. Rev. E* **94**, 052401 (2016).
18. C. Hartmann, Ö. Özmutlu, H. Petermeier, J. Fried, A. Delgado, Analysis of the flow field induced by the sessile peritrichous ciliate *Opercularia asymmetrica*. *J. Biomech.* **40**, 137–148 (2007).
19. A. J. Mathijssen, J. Culver, M. S. Bhamla, M. Prakash, Collective intercellular communication through ultra-fast hydrodynamic trigger waves. *Nature* **571**, 560–564 (2019).
20. C. Dombrowski, L. Cisneros, S. Chatkaew, R. E. Goldstein, J. O. Kessler, Self-concentration and large-scale coherence in bacterial dynamics. *Phys. Rev. Lett.* **93**, 2–5 (2004).
21. I. Tuval *et al*., Bacterial swimming and oxygen transport near contact lines. *Proc. Natl. Acad. Sci. U.S.A.* **102**, 2277–2282 (2005).
22. M. B. Short *et al*., Flows driven by flagella of multicellular organisms enhance long-range molecular transport. *Proc. Natl. Acad. Sci. U.S.A.* **103**, 8315–8319 (2006).
23. A. Andersen, T. Kiørboe, The effect of tethering on the clearance rate of suspension-feeding plankton. *Proc. Natl. Acad. Sci. U.S.A.* **117**, 30101–30103 (2020).
24. K. K. Christensen-Dalsgaard, T. Fenchel, Increased filtration efficiency of attached compared to free-swimming flagellates. *Aquat. Microb. Ecol.* **33**, 77–86 (2003).
25. R. A. Alegado *et al*., A bacterial sulfonolipid triggers multicellular development in the closest living relatives of animals. *eLife* **2012**, e00013 (2012).
26. T. Fenchel, Microbial behavior in a heterogeneous world. *Science* **296**, 1068–1071 (2002).
27. J. R. Blake, S. R. Otto, D. A. Blake, Filter feeding, chaotic filtration, and a blinking stokeslet. *Theor. Comput. Fluid Dyn.* **10**, 23–36 (1997).
28. B. A. Orme, S. R. Otto, J. R. Blake, Enhanced efficiency of feeding and mixing due to chaotic flow patterns around choanoflagellates. *IMA J. Math. Appl. Med. Biol.* **18**, 293–325 (2001).
29. T. Fenchel, R. N. Glud, Veil architecture in a sulphide-oxidizing bacterium enhances countercurrent flux. *Nature* **394**, 367–369 (1998).
30. A. Petroff, A. Libchaber, Hydrodynamics and collective behavior of the tethered bacterium *Thiovulum majus*. *Proc. Natl. Acad. Sci. U.S.A.* **111**, E537–E545 (2014).
31. A. P. Petroff, A. L. Pasulka, N. Soplop, X. L. Wu, A. Libchaber, Biophysical basis for convergent evolution of two veil-forming microbes. *R. Soc. Open Sci.* **2**, 2150437 (2015).
32. D. Ammermann, M. Schlegel, Characterization of two sibling species of the genus *Stylonychia* (Ciliata, Hypotricha): *S. mytilus* Ehrenberg, 1838 and *S. lemnae* n. sp. I. Morphology and reproductive behavior. *J. Protozool.* **30**, 290–294 (1983).
33. P. Madoni, Protozoa in wastewater treatment processes: A minireview. *Italian J. Zool.* **78**, 3–11 (2011).
34. W. E. Ranz, Applications of a stretch model to mixing, diffusion, and reaction in laminar and turbulent flows. *AIChE J.* **25**, 41–47 (1979).
35. E. Villermaux, Mixing versus stirring. *Annu. Rev. Fluid Mech.* **51**, 245–273 (2019).
36. N. Ricci, R. Giannetti, C. Miceli, The ethogram of *Euplotes crassus* (ciliata, hypotrichida): I. The wild type. *Eur. J. Protistol.* **23**, 129–140 (1988).
37. N. Ricci, Locomotion as a criterion to read the adaptive biology of protozoa and their evolution toward metazoa. *Boll. Zool.* **56**, 245–263 (1989).
38. J. R. Lawrence, R. A. Snyder, Feeding behaviour and grazing impacts of a Euplotes sp. On attached bacteria. *Can. J. Microbiol.* **44**, 623–629 (1998), 10.1139/w98-057.
39. H. C. Berg, *E. coli in Motion* (Springer, 2004).
40. N. Liron, S. Mochon, Stokes flow for a stokeslet between two parallel flat plates. *J. Eng. Math.* **10**, 287–303 (1976).
41. J. Ainley, S. Durkin, R. Embid, P. Boindala, R. Cortez, The method of images for regularized stokeslets. *J. Comput. Phys.* **227**, 4600–4616 (2008).
42. Z. Lin, J. L. Thiffeault, S. Childress, Stirring by squirmers. *J. Fluid Mech.* **669**, 167–177 (2011).
43. R. Cortez, D. Varela, A general system of images for regularized stokeslets and other elements near a plane wall. *J. Comput. Phys.* **285**, 41–54 (2015).
44. J. S. Guasto, R. Rusconi, R. Stocker, Fluid mechanics of planktonic microorganisms. *Annu. Rev. Fluid Mech.* **44**, 373–400 (2011).
45. K. Drescher, J. Dunkel, L. H. Cisneros, S. Ganguly, R. E. Goldstein, Fluid dynamics and noise in bacterial cell-cell and cell-surface scattering. *Proc. Natl. Acad. Sci. U.S.A.* **108**, 10940–10945 (2011).
46. G. Haller, Lagrangian coherent structures. *Annu. Rev. Fluid Mech.* **47**, 137–162 (2015).
47. A. Surana, O. Grunberg, G. Haller, Exact theory of three-dimensional flow separation. Part 1. Steady separation. *J. Fluid Mech.* **564**, 57–103 (2006).
48. R. S. MacKay, Transport in 3D volume-preserving flows. *J. Nonlinear Sci.* **4**, 329–354 (1994).
49. P. Meunier, E. Villermaux, The diffusive strip method for scalar mixing in two dimensions. *J. Fluid Mech.* **662**, 134–172 (2010).
50. F. Guzmán-Lastra, H. Löwen, A. J. Mathijssen, Active carpets drive non-equilibrium diffusion and enhanced molecular fluxes. *Nat. Commun.* **12**, 1906 (2021).
51. J. M. Ottino, *The Kinematics of Mixing: Stretching, Chaos, and Transport* (Cambridge University Press, 1989).
52. T. Tél, A. de Moura, C. Grebogi, G. Károlyi, Chemical and biological activity in open flows: A dynamical system approach. *Phys. Rep.* **413**, 91–196 (2005).
53. E. Gouillart, O. Dauchot, J. L. Thiffeault, Measures of mixing quality in open flows with chaotic advection. *Phys. Fluids* **23**, 1–12 (2011).
54. J. Heyman, D. R. Lester, R. Turuban, Y. Meheust, T. L. Borgne, Stretching and folding sustain microscale chemical gradients in porous media. *Proc. Natl. Acad. Sci. U.S.A.* **117**, 13359–13365 (2020).
55. M. Souzy, H. Lhuissier, E. Villermaux, B. Metzger, Stretching and mixing in sheared particulate suspensions. *J. Fluid Mech.* **812**, 611–635 (2017).
56. R. Turuban, D. R. Lester, T. L. Borgne, Y. Méheust, Space-group symmetries generate chaotic fluid advection in crystalline granular media. *Phys. Rev. Lett.* **120**, 024501 (2018).
57. D. Martínez-Ruiz, P. Meunier, B. Favier, L. Duchemin, E. Villermaux, The diffusive sheet method for scalar mixing. *J. Fluid Mech.* **837**, 230–257 (2018).
58. P. Meunier, E. Villermaux, The diffuselet concept for scalar mixing. *J. Fluid Mech.* **951**, A33 (2022).
59. R. Turuban, H. Lhuissier, B. Metzger, Mixing in a sheared particulate suspension. *J. Fluid Mech.* **916**, R4 (2021).
60. S. Shekhar *et al*., Cooperative hydrodynamics accompany multicellular-like colonial organization in the unicellular ciliate stentor. bioRxiv [Preprint] (2023). https://doi.org/10.1101/2023.01.10.523506 (Accessed 21 November 2024).
61. J. B. Kirkegaard, A. O. Marron, R. E. Goldstein, Motility of colonial choanoflagellates and the statistics of aggregate random walkers. *Phys. Rev. Lett.* **116**, 038102 (2016).
62. D. Blair, E. Dufresne, The matlab particle tracking code repository (2005). https://site.physics.georgetown.edu/matlab/.
63. R. Turuban, G. Noselli, A. Beran, A. DeSimone, Cooperative mixing in Stylonychia lemnae. SISSA Open Data. https://hdl.handle.net/20.500.12928/EP90AW. Deposited 22 August 2025.